Published in final edited form as:
Biochemistry. 2011 January 18; 50(2): 172–180. doi:10.1021/bi101365f.

Conformational Changes in IpaD from *Shigella flexneri* Upon Binding Bile Salts Provide Insight into the Second Step of Type III Secretion†

Nicholas E. Dickenson[1], **Lingling Zhang**[1,§], **Chelsea R. Epler**, **Philip R. Adam**, **Wendy L. Picking**, and **William D. Picking**[*]
Department of Microbiology and Molecular Genetics, Oklahoma State University, Stillwater, OK 74078

Abstract

Shigella flexneri uses its type III secretion apparatus (TTSA) to inject host-altering proteins into targeted eukaryotic cells. The TTSA is composed of a basal body and an exposed needle with invasion plasmid antigen D (IpaD) forming a tip complex that controls secretion. The bile salt deoxycholate (DOC) stimulates recruitment of the translocator protein IpaB into the maturing TTSA needle tip complex. This process appears to be triggered by a direct interaction between DOC and IpaD. Fluorescence spectroscopy and NMR spectroscopy are used here to confirm the DOC-IpaD interaction and to reveal that IpaD conformational changes upon DOC binding trigger the appearance of IpaB at the needle tip. Förster resonance energy transfer between specific sites on IpaD was used here to identify changes in distances between IpaD domains as a result of DOC binding. To further explore the effects of DOC binding on IpaD structure, NMR chemical shift mapping was employed. The environments of residues within the proposed DOC binding site and additional residues within the "distal" globular domain were perturbed upon DOC binding, further indicating that conformational changes occur within IpaD upon DOC binding. These events are proposed to be responsible for the recruitment of IpaB at the TTSA needle tip. Mutation analyses combined with additional spectroscopic analyses confirms that conformational changes in IpaD induced by DOC binding contribute to the recruitment of IpaB to the *S. flexneri* TTSA needle tip. These findings lay the foundation for determining how environmental factors promote TTSA needle tip maturation prior to host cell contact.

Keywords

Shigella; type III secretion; IpaD; DOC

†This work was supported through funding from NIH R01 AI067858 to WLP, R21 AI090149 to WDP and F32 AI084203 to NED.

[*]To whom correspondence should be addressed: Department of Microbiology and Molecular Genetics, Oklahoma State University, 307 Life Science East, Stillwater, OK 74078, Tel. 405-477-4600, Fax: 405-744-6790, william.picking@okstate.edu.
[1]The first two authors contributed equally to the work presented here.
[§]current address: Department of Molecular Biology, University of Texas Southwestern Medical Center, Dallas, TX 75390

Supporting Information Available. An ^{1}H-^{15}N TROSY-HSQC spectrum of IpaD$^{38–321}$ with its primary sequence assignment, an overlay of the ^{1}H-^{15}N TROSY-HSQC spectra of IpaD$^{38–321}$ containing specifically labeled amino acids, a comparative color-coded mapping of wild type and N146Q IpaD residues perturbed following DOC binding, an ^{1}H-^{15}N TROSY-HSQC spectrum of IpaD$^{38–321}$ prior to and following incubation with dehydrocholate, and an overlay of IpaD$^{38–321}$ and IpaD$^{38–321}$ N146Q ^{1}H-^{15}N TROSY-HSQC spectra are provided. A complete list of assigned residues and the corresponding chemical shift data prior to and following incubation with DOC are available for IpaD$^{38–321}$ and IpaD$^{38–321}$ N146Q. This material is available free of charge via the Internet at http://pubs.acs.org.

Shigella flexneri is the causative agent of shigellosis, a severe gastrointestinal syndrome with fever, abdominal pain, and diarrhea. There are an estimated 165 million cases of shigellosis worldwide each year, which results in over one million deaths with the most susceptible population being children under the age of four (1). While most shigellosis outbreaks can be linked to substandard water quality in developing countries (1), approximately 580,000 cases of shigellosis are reported in industrialized nations each year, especially in institutional settings such as daycares and nursing homes (2). Ominously, outbreaks are increasingly being accompanied by the identification of new antibiotic resistant strains (3).

Shigella spp. are transmitted by the fecal-oral route usually through contaminated water or fomites (4). Once consumed, the acid-tolerant bacteria pass through the upper gastrointestinal tract to the colonic mucosa where they are transcytosed by M cells into gut-associated lymphoid tissues. There they are phagocytized by macrophages from which they escape to the basolateral side of the colonic epithelium via bacterially induced apoptosis (5). The bacteria then invade the epithelial cells and escape into the cytoplasm where they move about using actin-based motility, which facilitates intercellular spread and subversion of the host immune system (4).

Shigella spp. use a type III secretion system (TTSS) to mediate communication between themselves and their eukaryotic hosts (6). The type III secretion apparatus (TTSA) provides the conduit for translocation of TTSS protein effectors from the bacterial cytoplasm to the host cell interior. The *S. flexneri* TTSA is a multi-protein assembly composed of a syringe-like basal body that spans the bacterial inner and outer membranes, an external needle composed of many copies of MxiH which extends beyond the LPS layer (7), and an associated needle tip complex composed of IpaD, IpaB, and IpaC (8–10). The tip complex matures in a stepwise manner to control type III secretion induction and ultimately promote bacterial entry into its eukaryotic host cell (10). Later effectors are injected into the host cell cytoplasm to further modify and fine-tune the host cell's response to invasion (11).

Docking of IpaD to the needle tip is the first step in needle-tip complex maturation since this is the only protein found at the TTSA needle tip of early log phase *Shigella* (8). Its localization at the tip is required for subsequent docking of IpaB and IpaC, which are ultimately needed to form the IpaB/IpaC translocon pore (8). Crystallized IpaD has a dumbbell shape with two globular domains flanking a central coiled-coil (12). The N-terminal globular domain consists of three short α-helices and computational modeling suggests that it resides adjacent to the TTSA needle once docked at the *Shigella* surface (12–13). The central coiled-coil provides structural integrity to the protein and interacts with MxiH to anchor IpaD to the needle tip (13–14). The globular "distal" domain consists of a few short α-helices and β-strands and is located most distant from the needle tip (9,12).

We have shown that when *S. flexneri* is incubated with deoxycholate (DOC) or other bile salts, IpaB is recruited to the TTSA needle tip to form a stable ternary complex consisting of MxiH, IpaD, and IpaB (9). Bile salts such as DOC are natural detergents within the human intestine and as such, they represent a potential environmental trigger for inducing IpaB recruitment to the TTSA needle tip as *Shigella* pass through the small intestine. Due to the hydrophobic nature of IpaB and its ability to interact with cholesterol and CD44 during the bacterial entry process (15–17), the presence of IpaB at the TTSA needle tip may be essential for bacterial sensing of the host cell membrane. Initial studies utilizing fluorescence spectroscopy and molecular modeling have suggested that DOC binds to a central region of the IpaD coiled-coil in the cleft formed between the coiled-coil and the N-terminal domain (18). In this study, we apply complementary spectroscopic techniques to examine the interaction between IpaD and DOC. The resulting data are consistent with DOC

binding near the middle of the IpaD coiled-coil, however, it appears that this binding results in conformational changes within IpaD. From these findings, we propose that environmentally-induced changes in IpaD structure contribute to the recruitment of IpaB to the TTSA needle tip and this sets the stage for the bacteria to sense host cell contact as a subsequent step in type III secretion induction.

Experimental Procedures

Materials

The *Shigella flexneri ipaD null strain* SF622 was provided by P. Sansonetti (Pasteur Institute, FR). Antibodies to IpaB and IpaD were provided by E. Oaks (Walter Reed Army Institute for Research, Silver Springs, MD). FlAsH-EDT_2, Alexa Fluor probes, and PCR Supermix High Fidelity were from Invitrogen (Carlsbad, CA). Oligonucleotide primers were purchased from Integrated DNA Technologies (Coralville, IA). *E. coli* strains, protein expression plasmids, and Clonables 2x Ligation Premix were from Novagen (Madison, WI). Restriction enzymes were from New England Biolabs (Ipswich, MA). ^{15}N-Ammonium chloride (99% pure), $^{13}C_6$-glucose (99% pure), ^{15}N L-Alanine (95–99%), ^{15}N L-Valine (95–99%), ^{15}N L-Leucine (95–99%), ^{15}N L-Isoleucine (95–99%), and deuterium oxide (D_2O, >99%) were from Cambridge Isotope Laboratories, Inc. (Andover, MA). Iminodiacetic acid-Sepharose and BME Vitamins solution were from Sigma Chemical Company (St. Louis, MO). All other solutions and chemicals were reagent grade.

Generation of plasmids for expression of ipaD mutant genes

IpaD point mutants were produced for use in complementation of *S. flexneri* or for protein expression as previously described (18). IpaD tetracysteine mutants were generated by inserting a tetracysteine (CCPGCC) binding pocket into specific sites on IpaD. Inverse PCR was used to make the mutant sequences of *ipaD* in pWPsf4 using specific primers as previously described (8). Primer sequences are available upon request. The plasmids were electroporated into the *Shigella ipaD* null strain SF622 for phenotypic characterization. The genes were also subcloned into pET15b, which was then used to transform *E. coli* Tuner(DE3) for protein production. For the NMR studies, a construct encoding residues 38–321 was produced and subcloned into pET22b for subsequent protein production.

Phenotypic characterization of S. flexneri SF622 expressing different ipaD mutants

The phenotype of each *ipaD* mutant in *Shigella* SF622 was determined using assays described previously (8,19). Invasion functions were monitored using a standard gentamycin-protection assay with cultured Henle 407 cells as described (20). The surface localization of IpaD and IpaB was determined by immunofluorescence microscopy as recently described (8–9).

Protein expression and purification

The *ipaD* tetracysteine mutants in pET15b were expressed as previously described (21). The fractions containing IpaD were dialyzed into 50mM HEPES (pH 7.5), 140mM NaCl, 10mM BME, and 1mM TCEP. For NMR studies, ^{15}N-labeled proteins were obtained by growing the expression strain in minimal media supplemented with ^{15}N-NH_4Cl as the nitrogen source. Uniformly ^{2}H-, ^{15}N-, ^{13}C-labeled proteins were obtained by growing the expression strain in minimal media prepared in D_2O and supplemented with ^{15}N-NH_4Cl and ^{2}H-, ^{13}C-glucose as the nitrogen and carbon sources, respectively. Recombinant protein was purified via His_6 tag by IMAC chromatography as described (21). Fractions were pooled and dialyzed into 10mM sodium phosphate buffer pH 7.0 with 10mM NaCl. For specific ^{15}N-amino acid proteins, IpaD was labeled using ^{15}N-labeled Leu, Val, Phe, Tyr, Ile, and Ala

individually. Briefly, the expression strain was grown in LB medium at 37°C overnight. The cells were centrifuged and resuspended in minimal media supplemented with ^{15}N-amino acid (Isotec) and the rest of the 19 unlabeled amino acids. The cells were allowed to grow in minimal media for 45 min and induced with IPTG. Recombinant proteins were purified as described above.

Labeling of IpaD with FlAsH-EDT$_2$ and Alexa Fluor 568

The CCPGCC tetracysteine binding pockets within the purified recombinant IpaD proteins were labeled with FlAsH using a modified version of the method described by Squier *et al.* (22). After dialyzing against 50mM HEPES (pH 7.5), 140mM NaCl, 10mM BME, and 1mM TCEP to ensure reduction of disulfide bonds, a 1.1 molar excess of FlAsH-EDT$_2$ reagent was added to the protein solution and allowed to react for 1 hour at room temperature and 24 hours at 4°C with gentle rocking. Excess FlAsH was removed by nickel chelation chromatography and the fractions analyzed by SDS-PAGE (12% gel) using a UV light source to observe the fluorescently labeled protein. Fractions containing FlAsH-labeled IpaD were pooled and reduced by adding BME to 10mM and TCEP to 1mM for 30 min at room temperature. The BME was removed by dialysis against 50mM HEPES (pH 7.0), 140mM NaCl, and 1mM TCEP. Alexa Fluor 568 maleimide in DMF was added in ~10 molar excess to an aliquot of the FlAsH-labeled IpaD protein. After gentle rocking for 1 hour at room temperature and 24 hours at 4°C, the unbound dye was removed by nickel chelation chromatography. The double-labeled protein was dialyzed into 50mM HEPES (pH 7.0), 140mM NaCl, and 1mM TCEP and either used immediately or stored at −80°C.

Fluorescence spectroscopy

Fluorescence emission spectra of IpaD were collected at 20°C with a FluoroMax-4 spectrofluorometer (HORIBA Jobin Yvon, Edison, NJ) using an excitation wavelength of 485nm and an emission wavelength range of 500–650nm with excitation and emission slit widths of 2.5nm and an integration time of 0.1 seconds. Fluorescence emission spectra of both donor only as well as donor and acceptor-labeled IpaD were collected prior to and following a 30 minute incubation with 1mM DOC at 20°C in order to observe the effects of DOC binding on IpaD conformation.

Calculating intramolecular distances of FRET pairs

Donor-acceptor distances were calculated using FRET efficiencies, which were measured spectrophotometrically and calculated by the change in intensity in donor fluorescence. Because the donor only sample was removed prior to labeling of the protein with the FRET acceptor, the FlAsH (donor) labeling efficiencies of the two samples are identical and the energy transfer efficiencies can be calculated by:

$$E=1-(F_{DA}/F_{D}) \quad \text{Eq.1}$$

where E is the energy transfer efficiency, F_{DA} is the peak fluorescence intensity of the donor emission in the presence of the acceptor and F_D is the peak fluorescence intensity of the donor emission in the absence of the acceptor fluorophore. Because of the detergent properties of DOC (which was used below its critical micelle concentration), resulting changes in fluorophore properties following DOC addition had to be taken into account. By measuring the donor fluorescence in both the presence and absence of acceptor prior to and following DOC incubation, the slight quenching effect of the DOC on the donor is accounted for in the calculations. A titration of up to 1mM DOC into acceptor-labeled IpaD resulted in a maximum change in extinction coefficient of the acceptor of 0.65%, which lies well within the acceptable range for this set of experiments.

From the energy transfer efficiencies, the distances between donor and acceptor dyes are calculated by:

$$r = R_0 * [(1/E) - 1]^{1/6} \quad \text{Eq.2}$$

where r is the distance between the FRET pair fluorophores, E is the measured energy transfer efficiency calculated from Eq.1, and R_0 is the Förster distance specific for the FRET pair. R_o value for FlAsH and Alexa Fluor 568 is 75Å (23).

Using NMR chemical shift perturbations to identify the interaction between IpaD and deoxycholate (DOC)

Uniformly ^{15}N-labeled IpaD$^{38–321}$ was purified and dissolved in NMR buffer (10mM sodium phosphate, pH 7.0, 10mM NaCl, 10% D_2O, and 90% H_2O). NMR data were acquired at 30°C on a Bruker Avance 800 MHz spectrometer fitted with a cryogenic triple-resonance probe and a Z-axis pulse field gradient. NMR data were processed using NMRPipe and analyzed using NMRView (24–25). A two-dimensional ^{1}H-^{15}N TROSY-HSQC (26) spectrum of free IpaD was collected, and then spectra of IpaD with DOC bound were acquired at DOC:IpaD molar ratios of 1, 3, and 6. IpaD residues with chemical shift perturbations were identified by overlaying the ^{1}H-^{15}N TROSY-HSQC spectra as described (14). Assignments of the backbone resonances were accomplished by collecting data on perdeuterated ^{15}N, ^{13}C-labeled IpaD$^{38–321}$ using 2D ^{1}H-^{15}N TROSY-HSQC and TROSY-based 3D HNCA and 3D HNCACB (26–28).

Results

Measurement of IpaD conformational changes through Förster resonance energy transfer

Based on previous intermolecular Förster resonance energy transfer (FRET) from IpaD to a fluorescein linked to DOC (18), it was proposed that DOC binds to IpaD within the cleft formed between α2 and α3 (Fig. 1). To determine whether this binding event is associated with a change in IpaD's structure, FRET was once again employed. Four unique IpaD mutants, each containing a single tetracysteine pocket (CCPGCC), were generated (see Fig. 2A) to allow specific coordination of a fluorescent FlAsH tag at known locations within the protein. As indicated by Equation 2, FRET exhibits the greatest sensitivity to conformational change when the donor/acceptor fluorophore pair is separated by a distance that is near the Förster distance specific for the dye pair. Based on the IpaD crystal structure and the locations of the fluorophore labeling sites, Alexa Fluor 568 was chosen to label the single cysteine of IpaD (Cys322) to serve as the FRET acceptor for the FlAsH label (due to the relatively large R_o value of 75Å).

In order to best maintain protein structure and stability, tetracysteine motifs were intentionally introduced into unstructured regions located between the stabilizing helices of IpaD. When the four tetracysteine-containing IpaD mutants were used to complement a *Shigella ipaD* null strain, they were all found to be invasive. Furthermore, labeling the IpaD tetracysteine mutants while in the live *S. flexneri* bacteria resulted in no reduction in invasiveness of the organisms, showing that the FlAsH coordination did not interfere with IpaD stability or function. Because phenotype could not be used to evaluate the influence of covalent addition of acceptor fluorophore to Cys322 of IpaD, both secondary and tertiary structure stability of the Alexa Fluor 568-labeled protein and its TC mutant forms were probed by monitoring thermal unfolding using CD and tryptophan fluorescence spectroscopies, respecitvely. In all cases, the thermal stability of the labeled protein was virtually identical to that of the unlabeled protein (data not shown). Together these data

indicate that the addition of the fluorescent probes necessary for the FRET experiments do not have a detrimental impact on protein structure or stability.

Energy transfer efficiency was determined by measuring donor fluorophore emission in the presence and absence of the FRET acceptor (Fig. 2C). The sensitivity of FRET to small changes in distance between donor and acceptor probes allows for detection of conformational changes within IpaD, which may occur upon the binding of DOC (Fig. 2C). Energy transfer from the donor to the acceptor in the dual-labeled protein resulted in a substantial decrease in the donor fluorescence intensity and the appearance of an emission peak from the acceptor fluorophore. The decrease in donor fluorescence resulting from the non-radiative transfer of energy to the acceptor was used to calculate the energy transfer efficiency, which was then used to calculate the distance between the FRET pair for each of the IpaD tetracysteine mutants in the absence and presence of DOC (Table 1). Briefly, for the mutant with the FlAsH label located in the N-terminal domain (TC68), a decrease in FRET efficiency from 80.2±0.6% to 75.0±0.8% was measured corresponding an increase in the intramolecular fluorophore distance of 3.0Å following incubation with DOC. The mutant with the FlAsH fluorophore located at the distal end of the protein between helices α3 and α4 (TC184) exhibited the largest change as the donor-acceptor FRET pair showed a change in FRET efficiency of over 20%, which suggested a distance change of 11.3Å toward each other following DOC binding. The apparent distance between the donor located at the juncture of helices α6 and α7 (TC264) and the acceptor increased 2.6Å as a result of incubation with DOC. Finally, the largely unstructured region of the distal domain was also labeled with a FlAsH donor (TC231) and was found to move 4.6Å closer to the Cys322 Alexa Fluor acceptor following binding of DOC. These results indicate that upon binding DOC, IpaD undergoes a readily detectable conformational change with the greatest effect seen for the region distally attached to helix α3 (TC184).

It should be noted that while the measured intramolecular distances given in Table 1 compare favorably with what would be expected based on the IpaD crystal structure (12,18), there is an inherent error to be considered when making FRET-based distance determinations in complex biological systems. Specifically, the random nature of the donor emission dipole orientation with the acceptor excitation dipole have prompted the use of an orientation factor value (κ^2) of 2/3 as is commonly done for solution-based biological FRET measurements (29). Furthermore, the distances actually being determined are between fluorescent probes rather than between the moieties to which they are linked, allowing for an uncertainty proportional to the distances of the fluorophores from the target. Nevertheless, because all of the major assumptions are expected to remain constant and the influence of DOC on fluorophore properties by DOC has been tested and accounted for, changes in distance calculated to occur upon ligand binding are expected to accurately reflect changes in protein structure within the sensitivity levels afforded by FRET. Thus, the findings presented in Table 1 do reflect an accurate assessment of the structural events that occur within IpaD following its association with DOC.

Identification of IpaD residues that are perturbed upon addition of deoxycholate (DOC)

NMR chemical shift mapping is a technique used to assess changes in the local microenvironment of specific residues of a protein upon interaction with a binding partner. The residues whose environments are affected by the binding interaction demonstrate an altered or perturbed chemical shift in their characteristic NMR signals. The residues that show chemical shift perturbations can be either directly involved in the binding event or be affected by the resulting conformational changes.

Backbone resonances for IpaD were assigned using ^{1}H-^{15}N TROSY-HSQC, TROSY-based three-dimensional HNCA and HNCACB as well as ^{15}N-specific amino acid labeling (26–

28,30). These multiple strategies allowed assignment of 201 of the 284 residues in the analyzed IpaD$^{38–321}$ (see Supplemental Figures S1 and S2). Addition of DOC to ^{15}N-labeled IpaD$^{38–321}$ resulted in chemical shift perturbations for several IpaD residues, examples of which are shown in Fig. 3A. Titration of DOC into ^{15}N-labeled IpaD$^{38–321}$ further exaggerated the movement of the already perturbed peaks on the ^{1}H-^{15}N TROSY-HSQC spectrum from their original positions, indicating that this interaction is occurring on the fast exchange NMR time scale (Fig. 3A) which is in agreement with the micromolar binding affinity previously estimated from fluorescence polarization experiments (18). Figure 3B highlights the residues perturbed upon binding of DOC with color-coding used to indicate the degree of perturbation for each residue. Many of the perturbed residues are located within the central coiled-coil of IpaD, which corresponds with the predicted DOC binding site identified by molecular modeling (see Fig. 1). Interestingly, several perturbed chemical shifts belong to residues that reside outside the predicted DOC binding pocket (Fig. 3B and Supplemental Table S1). For example, the characteristic signal of one tryptophan side chain was perturbed, indicating that one of the four Trp residues in IpaD is affected by DOC binding. From mutational analyses, it was determined that the perturbed Trp side chain belongs to W177 (data not shown). W177 is not located within the proposed binding pocket, but it is near the linker adjoining α3 and the distal domain, suggesting that DOC binding induces conformation changes in IpaD with exaggerated effects in this part of the protein. The positions of other residues outside the predicted DOC binding pocket are shown in Figure 3B and many of these lead up α3 and into the distal domain (Fig. 3B and Supplemental Table S1). These findings corroborate the FRET data showing that IpaD undergoes an overall conformational change as a result of DOC binding.

Mutagenesis studies indicate that IpaD residues affected by DOC binding are functionally important

Based on information revealed while solving the original crystal structure, there is a four residue region within helix α3 of the central coiled-coil of IpaD (residues 146–149) that retains only partial α-helical character and is thus capable of developing a kink (12). Such a region in α3 could contribute to conformational changes that occur as a result of DOC binding since this region is very near the proposed binding pocket. One of these residues (Y149) is influenced by DOC binding (see Fig. 3A and Supplemental Table S1). To investigate this further, the mutants N146Q, Y149F and N146Q/Y149F (Table 2) were generated because these mutations were expected to stabilize the α-helix and the reduced flexibility in this region could affect the structural dynamics and function of IpaD. If such structural dynamics are important for IpaD-mediated virulence functions, *Shigella* expressing these mutants would likely exhibit altered invasiveness. Indeed, the N146Q and Y149F mutations each resulted in nearly an 80% reduction in *Shigella* invasiveness and the N146Q/Y149F double mutant was noninvasive (Table 2). When the IpaD surface localization for Y149F and N146Q/Y149F was examined, little change from wild type was seen. Addition of DOC, however, resulted in a decrease in IpaD surface localization, especially in the double mutant strain (Table 2). Furthermore, these mutant strains were not capable of stably maintaining IpaB at the needle tip, which is consistent with the observed decrease in invasion function. The N146Q mutant strain presented a unique surface localization phenotype because regardless of whether grown in the presence or absence of DOC, IpaD localized at approximately wild type levels, however, IpaB was also on the surface in the absence of DOC (Table 2). This could indicate that the N146Q mutant adopts a conformational state that mimics the one caused by DOC binding, perhaps via stabilization of the α-helical character of α3. Therefore, IpaD N146Q (as opposed to Y149F or the double mutation) represents an especially interesting mutant (based on phenotype) that warranted further investigation.

NMR analysis of the IpaD N146Q mutant

To follow up phenotypic characterization of the α3 kink mutants, additional NMR experiments were used to understand the effect that this mutation has on DOC-induced conformational changes in IpaD. Accordingly, the ^{1}H, ^{15}N TROSY-HSQC spectrum of free ^{15}N-labeled IpaD$^{38–321}$ N146Q was compared with the spectrum of the same protein incubated with an equimolar amount of DOC (Fig. 4). The residues experiencing chemical shift perturbations in the coiled-coil DOC binding pocket of the N146Q mutant are similar to those of the wild-type IpaD, suggesting that DOC still binds to the same region on the mutant protein as in the wild type (Supplemental Tables S1 and S2 and Supplemental Figure S3). However, the globally decreased perturbations suggest that affinity for the DOC ligand may be reduced in the mutant. Furthermore, the N146Q point mutation caused the chemical shift perturbations for several residues outside of this region to show significantly reduced degrees of change when compared to those for IpaD not having the N146Q mutation (Supplemental Tables S1 and S2 and Supplemental Figure S3). This indicates that stabilization of the kink in α3 affects the degree of the conformational change that occurs within IpaD upon binding of DOC. Some of the residues exhibiting varying degrees of change are pointed out in Figure 4 where those most affected appear to cluster within helix α3, distal to the location of the kink in the native protein. This supports the idea that the kink has an important role in the structural and functional dynamics of IpaD as it relates to DOC binding.

FRET analysis of the IpaD N146Q mutant

Based on the NMR chemical shift data above, we introduced the N146Q mutation into each of the four tetracysteine pocket IpaD proteins described earlier in order to examine the FRET efficiency and change in distance separating the fluorophores following DOC binding (Table 3). Although the recombinant TC231/N146Q protein could be purified and fluorescently labeled, the combination of the N146Q point mutation and the tetracysteine insertion appeared to cause the protein to become misfolded based on CD spectroscopy and temperature dependent tryptophan emission data (data not shown). Thus, data for this mutant protein are not included in Table 3. When distance changes induced by DOC binding were considered, the IpaD TC68 N146Q mutant resulted in a change in distance of 3.1±0.8Å (the two probes moving away from each other) following the addition of 1mM DOC (Table 3), which is nearly identical to the relative change in probe position for the wild-type proteins (Table 1). Likewise, the addition of DOC to the TC264 version of the N146Q mutant exhibited a decrease in distance that was nearly identical to its wild-type counterpart (Tables 1 and 3). The reproducibility of the observed changes would argue that DOC induces a highly specific and consistent alteration on IpaD structure. Interestingly, when the TC184 N146Q mutant was investigated for the conformational effects of DOC binding, the apparent decrease in distance between donor and acceptor was only 6.1Å, which is substantially less than that seen for IpaD lacking the mutational change within the coiled-coil (11.3Å). The attenuation of the distance change here is consistent with the potential stabilization of the α3 “kink” giving rise to an intermediate structure that is able to assume a conformation that leads to IpaB recruitment to the TTSA needle tip. However, solving the crystal structures for native and N146Q IpaD in bound and unbound states will be necessary to fully characterize the global effects of not only DOC binding, but also the N146Q mutation itself.

Discussion

From its position at the tip of the *Shigella* TTSA needle, IpaD serves as a sensor of environmental factors to trigger the mobilization of the first translocator protein (IpaB) to the needle tip. This is consistent with IpaD’s known role in controlling *Shigella* type III

secretion (8,31). Previous biochemical, biophysical, and computational data have shown that IpaD binds bile salts and this is sufficient to promote the stable recruitment of IpaB to the TTSA needle tip without further induction of type III secretion (9,18). This marks the second step in the maturation of the TTSA needle tip complex. The mechanism by which small molecule ligands interact with IpaD to promote IpaB recruitment to the TTSA needle tip are not known, but allosteric effects on IpaD are most likely involved. To map potential conformational changes within IpaD that result from DOC binding and result in the recruitment of IpaB to the TTSA needle tip we employed complementary approaches that included FRET, NMR, and mutagenesis.

FRET studies were used first to monitor distance changes from Cys322, which is believed to reside near where IpaD contacts the TTSA needle, to specific sites at which FlAsH tags were coordinated. The resulting data indicated that DOC binding by IpaD results in a significant and reproducible conformational change that involves the most distal portion of IpaD moving as much as 11Å closer to an Alexa 568 acceptor probe on Cys322. In studies such as this, FRET provides a sensitive spectroscopic ruler, however, there are a limited number of locations to which the FlAsH binding motif could be inserted without compromising IpaD function and/or structure. This constraint prevents developing a full picture of the effects that DOC binding has on the structural dynamics of IpaD. In contrast, NMR spectroscopy can be used to monitor altered local environments of specific residues throughout IpaD upon ligand binding. NMR chemical shift mapping has previously provided valuable information of interactions occurring within the TTSA (14). A similar approach was used here to determine the IpaD residues that are affected by the binding of DOC. For these NMR studies, a new construct encoding $IpaD^{38–321}$ was designed based on the IpaD derivative used to solve its crystal structure (12).

More than two thirds of the residues for $IpaD^{38–321}$ were assigned using TROSY-based three-dimensional data (see Supplemental Materials). By using ^{1}H-^{15}N NMR chemical shift mapping, several IpaD residues were identified that were perturbed upon titrating in DOC (Fig. 3A and Supplemental Table S1). When mapped onto the IpaD crystal structure (Fig. 3B), it is clear that many of the affected residues reside within the proposed DOC binding site as expected, however, a substantial number of perturbed residues also appear throughout other parts of the protein. This is consistent with the FRET data showing that IpaD experiences some type of conformational changes outside of the pocket to which DOC is proposed to bind.

When the experimental data discussed thus far are considered, a pattern emerges that is consistent with computational models of DOC docking and the existence of consequential allosteric influences caused by this binding event. Key residues that are predicted to be involved in DOC binding using computational analyses, including K72, S82, and S86 in the N-terminal globular domain and L150, Y153, H155, S158 and T161 in α3 of the coiled-coil, showed prominent chemical shift perturbations in these experiments (see Supplemental Table S1). It is noteworthy, however, that a pattern of additional IpaD residues in α3 of the coiled-coil showed NMR chemical shift perturbations despite their location outside of the proposed DOC binding site. The residues on α3 that are notably perturbed by DOC binding extend up the helix to the distal domain and include F167, V170, S172, and S173 among others (Fig. 3). The short linker connecting the end of the α3 helix and the beginning of the distal domain, consisting of G176, W177, and I178, is also perturbed upon DOC binding. Many residues within the distal domain also displayed chemical shift changes, supporting the FRET data indicating that DOC binding induces a major conformational change that significantly influences residues within this region of IpaD.

Previous data agree with docking simulations that there is a single DOC binding site on α3 of the IpaD coiled-coil (18) and are consistent with the proposal that DOC induces structural changes in IpaD. Furthermore, the interaction between IpaD and DOC appear to be specific since a derivative of DOC (dehydrocholate) that is predicted not to bind to IpaD based on molecular modeling had little or no effect on the NMR spectrum of the protein (see Supplemental Figure S4), indicating that it does not cause a detectable conformational change in IpaD. It would thus appear that neither interactions between IpaD and generic small molecules nor non-specific detergent effects are likely. Rather, dynamic changes in the IpaD structure caused by specific DOC binding provide the most logical explanation for how environmental signals could lead to the recruitment of IpaB to the TTSA needle tip prior to host cell contact. Changes in IpaD structure could also account for the stable association of IpaB with the maturing needle tip complex following *Shigella* exposure to DOC since it is the distal domain that has been implicated in the stable maintenance of IpaB at the TTSA needle tip (12).

From these NMR data, it is proposed that α3 has a significant role in the conformational changes that ultimately influence the relative position of the distal domain of IpaD upon DOC binding and this, in turn, influences IpaD function. It is worth noting that residues N146 to Y149 of helix α3 have a reduced capacity to form an α-helix and thus they develop a kink within that part of the protein (12). This unusual feature of α3 could be contributing to the structural dynamics of IpaD and the conformational changes seen following DOC binding. This region was therefore targeted for introducing mutations that would be expected to stabilize the helical character of the region to see if this would interfere with the effect that DOC binding has on the structural changes observed within IpaD.

As shown in Table 2, mutations expected to stabilize the kink in α3 did influence the effect that DOC has on IpaD and IpaB presentation at the *Shigella* TTSA needle tip. For example, the IpaD N146Q mutation resulted in the detection of IpaB on the bacterial surface prior to adding DOC, suggesting that the mutation at N146 locks IpaD into a post-DOC binding conformation. These data indicate that the short kink in the middle of helix α3 could have a key role in the recruitment of IpaB to the tip of the *Shigella* TTSA needle tip. To extend these findings, NMR data were collected for the IpaD N146Q mutant in the absence and presence of DOC. DOC was still able to bind to the protein as indicated by the chemical shift perturbations for residues within the proposed DOC binding site, however, several residues outside of the proposed DOC binding pocket displayed attenuated perturbations (see Fig. 4 and Supplemental Materials). These data suggest that stabilization of α3 has little affect on the location of DOC binding, but there is an attenuated influence on specific residues outside the binding pocket that were affected by the ligand-induced conformational changes seen in wild-type IpaD after adding DOC. While DOC binding similarly affects the same binding site residues regardless of the kink, stabilizing the helix results in an altered conformational change involving the distal end of α3 (Supplemental Figure S3). While speculative, this is consistent with the FRET data collected for the IpaD N146Q mutant, which showed that stabilization of α3 results in an attenuation of the structural change seen after DOC addition (Table 3). A full understanding of the global structural effects of introducing the N146Q mutation to IpaD as well as the effects of DOC binding on the structures of the native IpaD and its N146Q mutant will probably require solving all of these crystal structures. Efforts are currently under way to do this to provide a high-resolution molecular snapshot of the proteins to precisely define the conformational changes that are identified in this study.

From previous molecular modeling and the experimental results presented here, we propose that IpaD undergoes a conformational change following the binding of DOC. Specifically, it is proposed that the flexibility in α3 is central to the conformational change observed here,

which in turn results in the global positioning of the various IpaD domains including the substantial change in the spatial relation of the region distal to helix α3 to the C-terminus. It is this overall structural change that allows IpaB to be recruited at the needle tip in a controlled manner. There are specific residues in IpaD that either interact with DOC directly or are involved in conformational changes following DOC binding as determined by NMR spectroscopy and FRET analyses. It is thus proposed that DOC, and perhaps other small molecule ligands in the human intestine, are able to induce conformational changes in IpaD that allow the controlled release of IpaB to give rise to a MxiH-IpaD-IpaB ternary complex. It is this complex that then triggers further type III secretion induction upon host cell contact (10). The fact that tip complex proteins are known to exist in a broad range of pathogens harboring TTSSs suggests that similar sensory functions can be used for type III secretion induction for other important bacterial pathogens.

Supplementary Material

Refer to Web version on PubMed Central for supplementary material.

Acknowledgments

We acknowledge valuable discussions with Dr. R. De Guzman (University of Kansas). Dr. Gerald Lushington (Molecular Modeling Laboratory, University of Kansas) performed the molecular modeling and docking analyses.

Abbreviations

HSQC	heteronuclear single quantum coherence
TROSY	transverse relaxation optimized spectroscopy
IpaD	invasion plasmid antigen D
IpaB	invasion plasmid antigen B
TTSS	type III secretion system
TTSA	type III secretion apparatus
FRET	Förster resonance energy transfer
MxiH	major exporter of Ipa proteins
DOC	deoxycholate
FlAsH	4′,5′-bis(1,3,2,-dithioarsolan-2-yl) fluorescein
TCEP	tris(2-carboxyethyl)phosphine

References

1. Niyogi SK. Shigellosis. J Microbiol. 2005; 43:133–143. [PubMed: 15880088]
2. Mohle-Boetani JC, Stapleton M, Finger R, Bean NH, Poundstone J, Blake PA, Griffin PM. Communitywide shigellosis: control of an outbreak and risk factors in child day-care centers. Am J Public Health. 1995; 85:812–816. [PubMed: 7762715]
3. Wong MR, Reddy V, Hanson H, Johnson KM, Tsoi B, Cokes C, Gallagher L, Lee L, Plentsova A, Dang T, Krueger A, Joyce K, Balter S. Antimicrobial resistance trends of Shigella serotypes in New York City, 2006–2009. Microb Drug Resist. 2010; 16:155–161. [PubMed: 20438349]
4. Schroeder GN, Hilbi H. Molecular pathogenesis of *Shigella* spp.: controlling host cell signaling, invasion, and death by type III secretion. Clin Microbiol Rev. 2008; 21:134–156. [PubMed: 18202440]

5. Zychlinsky A, Prevost MC, Sansonetti PJ. *Shigella flexneri* induces apoptosis in infected macrophages. Nature. 1992; 358:167–169. [PubMed: 1614548]
6. Galan JE, Wolf-Watz H. Protein delivery into eukaryotic cells by type III secretion machines. Nature. 2006; 444:567–573. [PubMed: 17136086]
7. Deane JE, Roversi P, Cordes FS, Johnson S, Kenjale R, Daniell S, Booy F, Picking WD, Picking WL, Blocker AJ, Lea SM. Molecular model of a type III secretion system needle: Implications for host-cell sensing. Proc Natl Acad Sci U S A. 2006; 103:12529–12533. [PubMed: 16888041]
8. Espina M, Olive AJ, Kenjale R, Moore DS, Ausar SF, Kaminski RW, Oaks EV, Middaugh CR, Picking WD, Picking WL. IpaD Localizes to the Tip of the Type III Secretion System Needle of *Shigella flexneri*. Infect Immun. 2006; 74:4391–4400. [PubMed: 16861624]
9. Olive AJ, Kenjale R, Espina M, Moore DS, Picking WL, Picking WD. Bile salts stimulate recruitment of IpaB to the *Shigella flexneri* surface, where it colocalizes with IpaD at the tip of the type III secretion needle. Infect Immun. 2007; 75:2626–2629. [PubMed: 17296762]
10. Epler CR, Dickenson NE, Olive AJ, Picking WL, Picking WD. Liposomes recruit IpaC to the *Shigella flexneri* type III secretion apparatus needle as a final step in secretion induction. Infect Immun. 2009; 77:2754–2761. [PubMed: 19433542]
11. Ogawa M, Handa Y, Ashida H, Suzuki M, Sasakawa C. The versatility of *Shigella* effectors. Nature reviews. 2008; 6:11–16.
12. Johnson S, Roversi P, Espina M, Olive A, Deane JE, Birket S, Field T, Picking WD, Blocker AJ, Galyov EE, Picking WL, Lea SM. Self-chaperoning of the Type III Secretion System Needle Tip Proteins IpaD and BipD. J Biol Chem. 2007; 282:4035–4044. [PubMed: 17077085]
13. Espina M, Ausar SF, Middaugh CR, Picking WD, Picking WL. Spectroscopic and Calorimetric Analyses of Invasion Plasmid Antigen D (IpaD) from *Shigella flexneri* Reveal the Presence of Two Structural Domains. Biochemistry. 2006; 45:9219–9227. [PubMed: 16866368]
14. Zhang L, Wang Y, Olive AJ, Smith ND, Picking WD, De Guzman RN, Picking WL. Identification of the MxiH needle protein residues responsible for anchoring invasion plasmid antigen D to the type III secretion needle tip. J Biol Chem. 2007; 282:32144–32151. [PubMed: 17827155]
15. Hayward RD, Cain RJ, McGhie EJ, Phillips N, Garner MJ, Koronakis V. Cholesterol binding by the bacterial type III translocon is essential for virulence effector delivery into mammalian cells. Mol Microbiol. 2005; 56:590–603. [PubMed: 15819617]
16. Lafont F, Tran Van Nhieu G, Hanada K, Sansonetti P, van der Goot FG. Initial steps of *Shigella* infection depend on the cholesterol/sphingolipid raft-mediated CD44-IpaB interaction. Embo J. 2002; 21:4449–4457. [PubMed: 12198147]
17. Skoudy A, Mounier J, Aruffo A, Ohayon H, Gounon P, Sansonetti P, Tran Van Nhieu G. CD44 binds to the *Shigella* IpaB protein and participates in bacterial invasion of epithelial cells. Cell Microbiol. 2000; 2:19–33. [PubMed: 11207560]
18. Stensrud KF, Adam PR, La Mar CD, Olive AJ, Lushington GH, Sudharsan R, Shelton NL, Givens RS, Picking WL, Picking WD. Deoxycholate interacts with IpaD of Shigella flexneri in inducing the recruitment of IpaB to the type III secretion apparatus needle tip. J Biol Chem. 2008; 283:18646–18654. [PubMed: 18450744]
19. Kenjale R, Wilson J, Zenk SF, Saurya S, Picking WL, Picking WD, Blocker A. The needle component of the type III secreton of *Shigella* regulates the activity of the secretion apparatus. J Biol Chem. 2005; 280:42929–42937. [PubMed: 16227202]
20. Picking WL, Coye L, Osiecki JC, Barnoski Serfis A, Schaper E, Picking WD. Identification of functional regions within invasion plasmid antigen C (IpaC) of *Shigella flexneri*. Mol Microbiol. 2001; 39:100–111. [PubMed: 11123692]
21. Picking WL, Nishioka H, Hearn PD, Baxter MA, Harrington AT, Blocker A, Picking WD. IpaD of *Shigella flexneri* is independently required for regulation of Ipa protein secretion and efficient insertion of IpaB and IpaC into host membranes. Infect Immun. 2005; 73:1432–1440. [PubMed: 15731041]
22. Chen B, Mayer MU, Markillie LM, Stenoien DL, Squier TC. Dynamic motion of helix A in the amino-terminal domain of calmodulin is stabilized upon calcium activation. Biochemistry. 2005; 44:905–914. [PubMed: 15654746]

23. Granier S, Kim S, Shafer AM, Ratnala VR, Fung JJ, Zare RN, Kobilka B. Structure and conformational changes in the C-terminal domain of the beta2-adrenoceptor: insights from fluorescence resonance energy transfer studies. J Biol Chem. 2007; 282:13895–13905. [PubMed: 17347144]
24. Johnson KN, Tang L, Johnson JE, Ball LA. Heterologous RNA encapsidated in Pariacoto virus-like particles forms a dodecahedral cage similar to genomic RNA in wild-type virions. J Virol. 2004; 78:11371–11378. [PubMed: 15452258]
25. Delaglio F, Grzesiek S, Vuister GW, Guang Z, Pfeifer J, Bax A. NMRPipe: A multidimensional spectral processing system based on UNIX pipes. J Biomol NMR. 1995; 6:277–203. [PubMed: 8520220]
26. Czisch M, Boelens R. Sensitivity enhancement in the TROSY experiment. J Magn Reson. 1998; 134:158–160. [PubMed: 9740742]
27. Salzmann M, Wider G, Pervushin K, Senn H, Wuthrich K. TROSY-type triple resonance experiments for sequential NMR assignments of large proteins. J Am Chem Soc. 1999; 121:844–848.
28. Salzmann M, Pervushin K, Wider G, Senn H, Wuthrich K. TROSY in triple-resonance experiments: new perspectives for sequential NMR assignment of large proteins. Proc Natl Acad Sci U S A. 1998; 95:13585–13590. [PubMed: 9811843]
29. Lakowicz, JR. Principles of Fluorescence Spectroscopy. Plenum Press; New York: 1983.
30. Pervushin K, Riek R, Wider G, Wuthrich K. Attenuated T2 relaxation by mutual cancellation of dipole-dipole coupling and chemical shift anisotropy indicates an avenue to NMR structures of very large biological macromolecules in solution. Proc Natl Acad Sci U S A. 1997; 94:12366–12371. [PubMed: 9356455]
31. Menard R, Sansonetti P, Parsot C. The secretion of the *Shigella flexneri* Ipa invasins is activated by epithelial cells and controlled by IpaB and IpaD. Embo J. 1994; 13:5293–5302. [PubMed: 7957095]

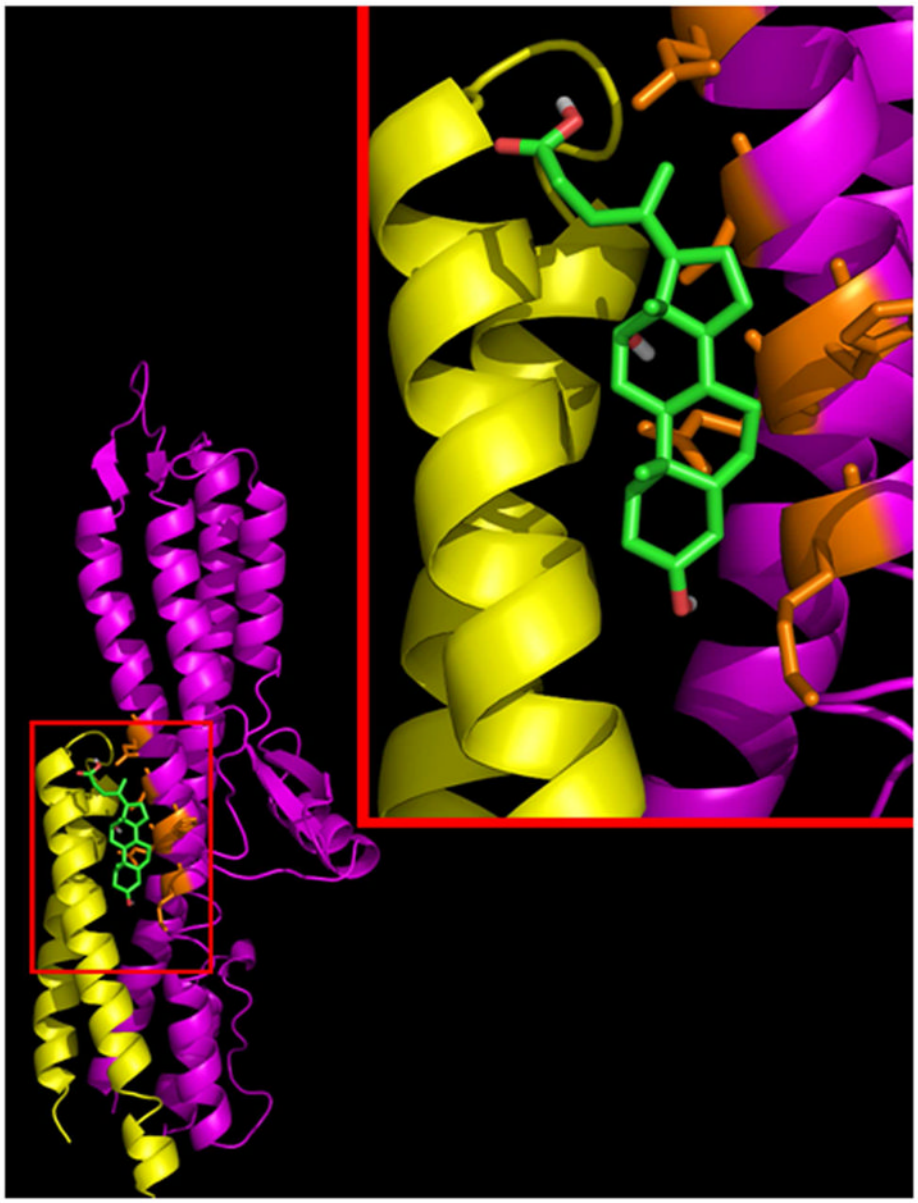

Figure 1. Computational (simulated) docking of deoxycholate (DOC) onto the crystal structure of IpaD

The ribbon structure of IpaD is shown in magenta, the ribbon structure of MxiH is shown in yellow and the structure of DOC is shown in green. DOC was docked onto the ribbon structure of IpaD using AutoDock (18). DOC is bound to the middle pocket of IpaD's coiled-coil where the head domain of MxiH packs against IpaD. Note that the docking simulation utilized the existing crystal structure of IpaD in the absence of DOC in order to identify the putative DOC binding site and the specific residues involved in the interaction. Thus they do not reflect any proposed conformational change in the protein following DOC binding. Inset: Enlarged view of the binding pocket showing key residues of IpaD (E154, H155, and S158) in orange that are essential for the interaction. (Reprinted with permission from the American Society for Microbiology. *Microbe*, December 2009, **4**:554–559)

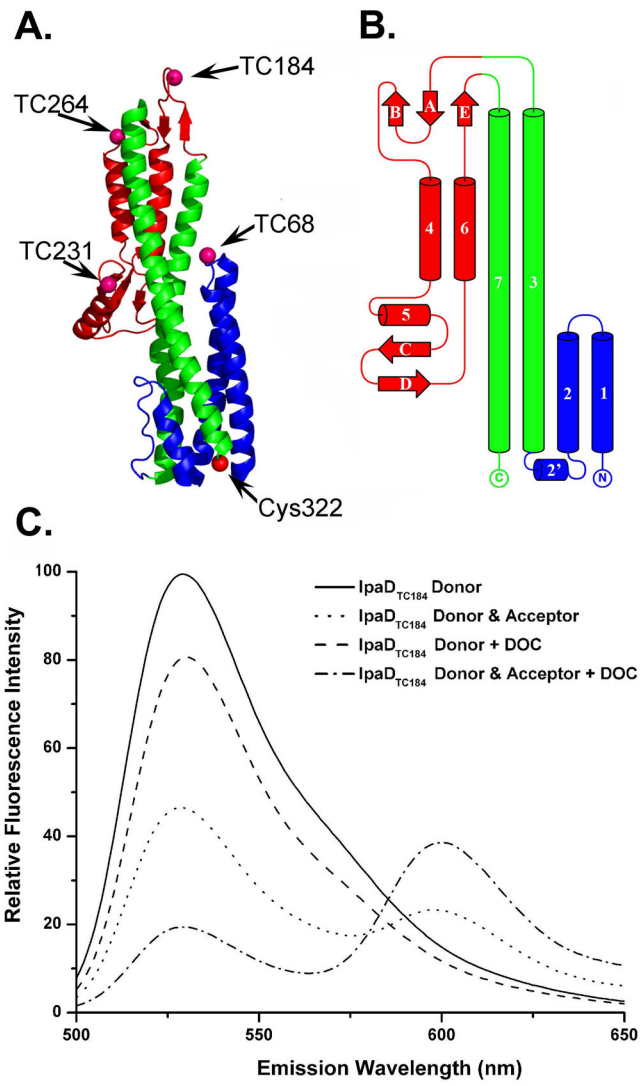

Figure 2. Location of tetracysteine (TC) pockets introduced into IpaD and FRET from FlAsH on TC184 to Alexa 568 on Cys322

Introduction of TC pockets was required to allow for site-specific FlAsH labeling. In **A**, the residues at which TC pockets were introduced are indicated on the ribbon structure of IpaD. The N-terminal domain is shown in blue, the central coiled-coil is green, and the distal domain is red. **B** is a cartoon depiction of IpaD in which the identifying numbers of the secondary structures are identified. In **C**, the emission spectra are shown of the IpaD TC184 mutant labeled with donor (FlAsH) alone or donor and acceptor (Alexa 568) in the absence and presence of 1mM DOC. The key for identification of each spectrum is given as part of the inset.

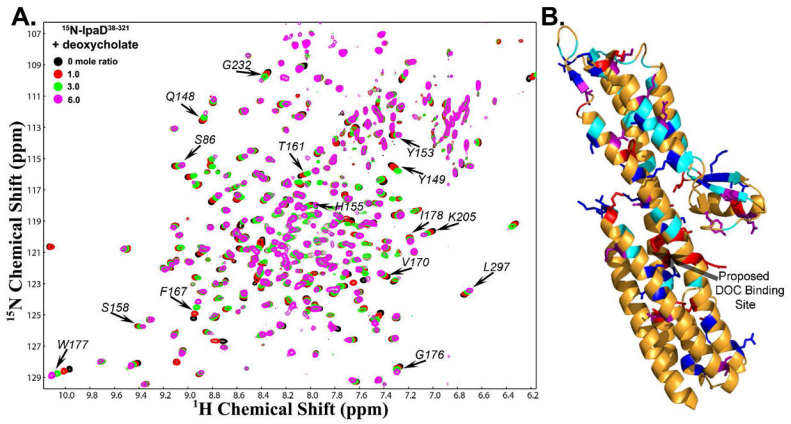

Figure 3. Titration of ^{15}N-labeled IpaD$^{38–321}$ with increasing amounts of DOC

In **A**, an overlay of four protein-nitrogen correlation spectra (^{1}H, ^{15}N TROSY-HSQC) at various DOC:IpaD molar ratios (black, 0; red, 1.0; green, 3.0; magenta, 6.0) is shown. The actual DOC:IpaD concentrations used, respectively, are as follows (in μM): black (500:0), red (500:500), green (500:1500), and magenta (500:3000). In **B**, the ribbon structure of IpaD is shown in orange, and the perturbed residues (listed in Supplemental Table S1) are color-coded based on degree of overall chemical shift perturbation seen for the backbone resonances following DOC binding (molar ratio = 6.0). Cyan, blue, magenta, and red represent residues observed to undergo combined chemical shifts between 0.01 and 0.10ppm, 0.10 and 0.20ppm, 0.20 and 0.30ppm, and greater than 0.30ppm, respectively. The proposed DOC binding site is indicated with the labeled arrow.

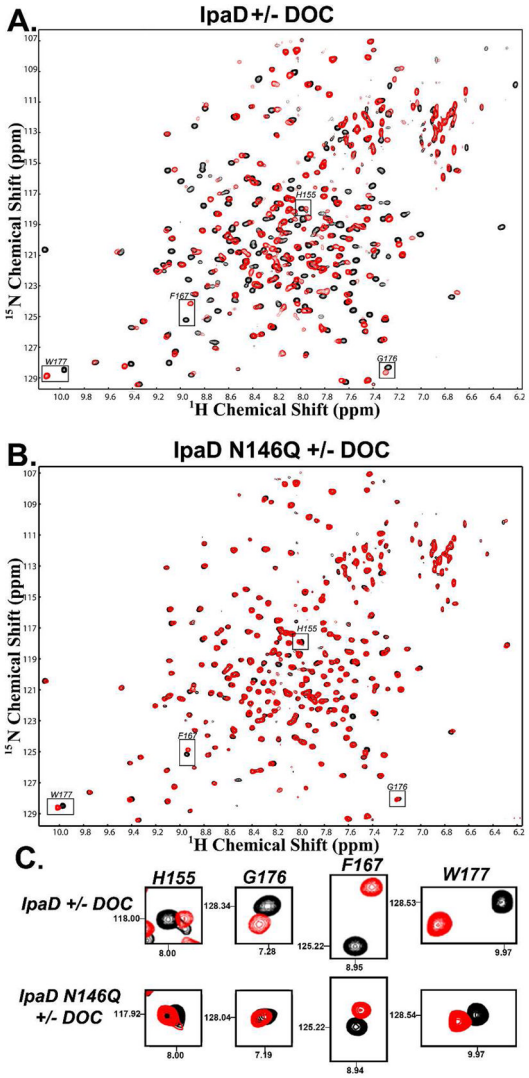

Figure 4. Incubation of ^{15}N-labeled IpaD$^{38–321}$ mutants with bile salts

^{1}H, ^{15}N TROSY-HSQC spectra of free ^{15}N-labeled wild-type IpaD$^{38–321}$ (**A**) or the IpaD N146Q mutant (**B**) (each shown in black) was overlaid with that of ^{15}N-labeled wild-type IpaD$^{38–321}$ or the IpaD N146Q mutant incubated with a 6:1 molar ratio of ratio of DOC:IpaD (each shown in red). The chemical shifts of some IpaD residues were perturbed similarly for each IpaD protein upon the binding of DOC, and these are mostly localized in the proposed binding pocket (e.g. H155). Some chemical shift perturbations caused by DOC binding appeared to be attenuated for the IpaD N146Q mutant and these tended to be within α3 as it approached the linker to the distal domain (e.g. F167, G176, and W177) (see inserts at **bottom**).

Table 1

Energy Transfer between FlAsH and Alexa Fluor 568 at Cys322.

		Native IpaD		IpaD+DOC		
FlAsH Site[a]	**Intramolecular Dist.(Å)**[b]	**%FRET Eff.**[c]	**Dist.(Å)**[d]	**%FRET Eff.**[c]	**Dist.(Å)**[d]	**Δ r(Å)**[e]
TC68	41.6	80.2±0.6	59	75.0±0.8	63	−3.0±0.8
TC184	78.6	54.0±0.7	73	75.9±0.6	62	+11.3±0.3
TC231	42.7	88.5±1.5	53	82.5±2.9	58	−4.6±1.9
TC264	74.7	51.4±2.0	74	56.7±1.2	72	+2.6±0.5

[a] Location of the tetracysteine pocket where the FlAsH coordinates.

[b] Distance between the tetracysteine pocket and Cys322 based on the crystal structure.

[c] The FRET efficiency is calculated as described in methods (n≥5 independent measurements).

[d] The calculated distance between FlAsH and Alexa Fluor 568 based on FRET measurements. Due to the assumptions required for calculating the distance between probes (discussed in the results section), the intramolecular distances are for reference only and are reported to within an estimated error of 1Å.

[e] The change in distance between the fluorophores after addition of DOC. The changes in energy transfer efficiencies resulting from DOC-induced conformational changes in IpaD are relative to the unbound state and therefore allow for calculating distance changes with greater accuracy than is possible for the absolute distances between the probes. Therefore, Δr is reported to a 0.1Å level of precision.

Table 2

The effect of selected IpaD mutations on *Shigella* invasiveness and surface localization of IpaD and IpaB.

		IpaD exposed(%)[b]		IpaB exposed(%)[c]	
IpaD mutant	**Relative invasion[a]**	**−DOC**	**+DOC**	**−DOC**	**+DOC**
ipaD null strain (SF622)	0±0	0±0	2±3	2±2	6±10
Wild type	100±8	78±11	92±13	0±0	84±9
N146Q	21±3	88±4	90±1	86±7	66±7
Y149F	23±8	93±7	77±23	13±9	41±6
N146Q/Y149F	4±3	87±6	21±1	13±7	1±2

[a] Invasion was measured using a standard gentamycin protection assay with the *S. flexneri ipaD* null strain SF622 serving as a negative control and SF622 expressing wild-type IpaD serving as a positive control and having 74±6 colonies per well (n=3).

[b] Surface exposed IpaD was detected using monoclonal antibodies while

[c] surface exposed IpaB was detected using rabbit antisera. In both cases, the value given is the percentage of cells having the given protein on the surface. The data shown are from a representative experiment that was performed in triplicate (n=3).

Table 3

Energy Transfer between FlAsH and Alexa Fluor 568 at Cys322 of IpaD N146Q.

	Native IpaD		IpaD+DOC		
FlAsH Site[a]	**%FRET Eff.**[b]	**Dist.(Å)**[c]	**%FRET Eff.**[b]	**Dist.(Å)**[c]	**Δr(Å)**[d]
TC68	74.3±1.9	63	68.5±0.8	66	−3.1±0.8
TC184	52.0±3.4	74	64.4±3.6	68	+6.1±0.8
TC264	43.4±1.9	78	48.4±4.0	76	+2.6±0.4

[a] Location of the tetracysteine pocket where the FlAsH coordinates.

[b] The FRET efficiency is calculated as described in methods (n≥5 independent measurements).

[c] The calculated distance between FlAsH and Alexa Fluor 568 based on FRET measurements. Due to the assumptions required for calculating absolute distances (discussed in the results section), the intramolecular distances are for reference only and are reported to an estimated error of 1Å.

[d] The change in distance between the fluorophores after addition of DOC. The changes in energy transfer efficiencies resulting from DOC-induced conformational changes in IpaD are relative to the unbound state and therefore allow for calculating distance changes with greater accuracy than is possible for the absolute distances between the probes. Therefore, Δr is reported to a 0.1Å level of precision.